

https://dspace.org/

Shock wave propagation into a valley

Whitehouse, Joanne

2006-10-30T12:16:13Z
http://hdl.handle.net/10539/1500

Downloaded from a DSpace repository. https://dspace.org/

DECLARATION

I, the undersigned, declare that this project report is my own, unaided work, except where otherwise acknowledged. It is submitted for the degree in Master of Science in Engineering in the University of the Witwatersrand, Johannesburg. It has not been submitted before for any degree or examination at any other university.

Signed this _____ day of _____ 20_____

Joanne Lyn Whitehouse

_____

ABSTRACT

An aircraft travelling at supersonic speeds close to the ground generates a bow wave, which is reflected off the ground surface. When the aircraft enters a valley, the three-dimensional bow wave is reflected off the valley walls, such that it could focus behind the aircraft. Complex three-dimensional wave surfaces will result. The real situation of an aircraft entering a valley can be modelled and tested experimentally in a shock tube. To simulate the process a planar shock wave, generated in a shock tube, is moved over several notched wedge configurations. Schlieren photographs were produced to identify the resulting complex three-dimensional wave structures and then verified by three-dimensional CFD. The valley geometries investigated are rectangular, triangular, parabolic and conical. Three hill geometries were also investigated.

The three-dimensional reflected surfaces from the rectangular valleys were found to vary only slightly as the valley floor inclination is increased. As the incident wave interacts with both the wedge and valley floor surfaces two prominent reflections occur. A primary reflected wave surface is generated from regular reflection off the wedge. This surface flows over into the valley contacting the incident wave at a second contact point. A secondary reflected wave is found underneath the primary reflected wave, generated due to Mach reflection occurring over the full width off the valley floor. The area of the incident wave between the second contact point and the triple point is seen to bow out into the downstream flow. The Mach stem of the reflection off the valley floor tends to become less pronounced for the larger valley floor inclination angles. In all the rectangular valleys, a shear layer is present, cascading down the valley wall and then along the valley entrance. The shear layer tends to decrease in size as the valley floor inclination increases. Both prominent reflected shock surfaces are almost conical in nature at close proximity to the valley wall.

The triangular valleys show similar reflection patterns as the rectangular valleys. As the incident shock wave initially interacts with the wedge surface only regular reflection occurs. The resulting reflected wave forms the primary reflected surface which flows over into the valley. The reflection changes to Mach reflection as the incident wave interacts with the valley floor. The Mach stem of the reflection off the valley floor increases in characteristic height as one moves from the valley entrance wall to the plane of symmetry. The Mach stem is much smaller for the higher valley floor inclinations. A secondary reflected wave is found underneath the primary reflected surface. The secondary wave is Mach reflection near the plane of symmetry which turns

to regular reflection closer to the valley wall. The primary and secondary reflected surfaces merge near the plane of symmetry and again along the wedge surface. A shear layer is found to cascade down the valley entrance wall for all geometries, decreasing in strength as the valley inclination angle increases.

The parabolic valleys show similar reflection patterns as the triangular valleys. As the incident wave interacts with both the wedge and valley surfaces two reflections occur. The reflection off the wedge surface is regular. As the incident wave flows over into the valley the initial reflection off the valley floor is regular. This regular reflection then turns into Mach reflection the closer one moves to the symmetry plane. The Mach reflection off the valley floor forms a secondary reflected wave underneath the primary reflected wave that is found to flow over into the valley. The primary reflected wave contacts the incident wave at a second contract point found above the triple point. This contact point moves closer to the triple point and eventually along the secondary reflected wave as the incident wave advances downstream. The second contact point at a single time instant is also seen to move closer to the triple point as one moves closer to the plane of symmetry. A shear layer is found cascading down the valley entrance wall. The secondary reflected wave of the Mach reflection off valley floor forms a semi-circular surface which contacts the floor just after the shear layer. The Mach reflection off the valley floor changes to regular reflection as the surface begins to climb up along the valley entrance wall.

The conical valleys once again show similar reflection patterns as those found in the other valley geometries. As the incident wave interacts with both the wedge and valley surfaces two reflections occur. Regular reflection occurs off the wedge surface with the resulting primary reflected wave flowing over into the valley. This primary reflected wave contacts the incident shock at a second contact point in the valley. The reflection off the valley floor is regular close to the valley entrance wall changing to Mach reflection nearer the symmetry plane. The reflected wave from the Mach reflection forms the secondary reflected surface found beneath the primary reflected wave. The secondary reflected Mach wave changes to regular reflection as the surface nears the valley wall, with the reflection point travelling along the valley floor until coincident with the valley entrance wall, where it then travels along the entrance wall. The second contact point found on the incident wave is found above the triple point and moves down the incident shock to eventually coincide with the triple point. A weak shear layer is found to cascade down the valley entrance wall. A weak separation also occurs at the entry point of the valley.

The three hill geometries, triangular, parabolic and conical, all display similar reflection patterns. As the incident wave advances downstream regular reflection occurs off both the wedge and hill surfaces. The reflected waves come together at a point off the surface. At this point a double triple point occurs with two resulting Mach stems. One Mach stem contacts the wedge surface while the other contacts the hill surface. The resulting double Mach stem surface wraps around the base of the hill getting progressively tighter the closer it gets to the incident wave. The only major differences between all three geometries is the shape of the resulting reflected wave off the hill surface (which tends to follow the same geometric shape as the hill) and the distance between the two triple points for the conical and parabolic hills tends to be larger than that found for the triangular hill.

This is dedicated to my family.

Thank-you for all your love and support.

ACKNOWLEDGEMENTS

I would like to express my sincere thanks Professor B. Skews for his unwavering advice, support and guidance throughout the duration of the project as well as for giving me the opportunity to present my work at the 25th International Symposium on Shock Waves.

I would like to thank Mr. J. Cooper, Mr D. Smith and all the laboratory and workshop staff of the School of Mechanical Engineering Laboratory at the University of the Witwatersrand, who manufactured my test pieces and for all their help during the duration of the project.

I would also like to thank Mr A. Andries and Mr N. Menon for their assistance with the optical system. I would also like to thank Mr G. Li for all his assistance during testing.

CONTENTS

DECLARATION ..... **i**
ABSTRACT ..... **ii**
ACKNOWLEDGEMENTS ..... **vi**
CONTENTS ..... **vii**
LIST OF FIGURES ..... **x**
LIST OF TABLES ..... **xiv**
NOMENCLATURE ..... **xv**
DEFINITION OF AXES ..... **xvi**

1 INTRODUCTION **1**
1.1 Background **1**
1.2 Shock wave reflection phenomena **3**
1.3 Literature review **5**
1.4 Motivation **12**
1.5 Objectives **12**
1.5.1 Experimental work 12
1.5.2 Numerical work 13
1.5.3 Comparison of experimental and numerical work 13

2 EXPERIMENTAL FACILITIES **15**
2.1 The Seitz shock tube **15**
2.1.1 Background 15
2.1.2 The shock tube facility 15
2.2 Data acquisition system and instrumentation **21**
2.2.1 Data acquisition system 21
2.2.2 Pressure and temperature measurements 21
2.3 Operation of the shock tube **22**
2.4 The optical system **23**
2.4.1 Distinction between Shadowgraph and Schlieren methods 23
2.4.2 Shadowgraph technique 23
2.4.3 Schlieren technique 23
2.4.4 The experimental optical system 24

2.5 The test pieces **25**
2.5.1 Test pieces requirements 26
2.5.2 Test pieces 26

3 EXPERIMENTAL AND COMPUTATIONAL PROCEDURES **32**
3.1 Testing procedure **32**
3.2 Developing procedure **33**
3.3 Experimental precautions **34**
3.3.1 Shock tube operating precautions 34
3.3.2 Film developing precautions 34
3.4 Computational Fluid Dynamics (CFD) modelling of the flow fields **35**
3.5 Development of the three-dimensional model **36**

4 PRESENTATION AND DISCUSSION OF EXPERIMENTAL AND COMPUTATIONAL RESULTS **38**
4.1 Experimental results overview **38**
4.2 Computational results overview **38**
4.3 Rectangular valley results **39**
4.3.1 Rectangular valley, $\theta_w = 60°$, $\theta_v = 0°$ 39
4.3.2 Summary of results for various rectangular valley configurations 49
4.4 Triangular valley results **55**
4.4.1 Triangular valley, $\theta_w = 60°$, $\theta_v = 0°$ 55
4.4.2 Summary of results for various triangular valley configurations 63
4.5 Parabolic valley results **68**
4.5.1 Parabolic valley, a = 0.04 68
4.5.2 Summary of results for various parabolic valley configurations 73
4.6 Conical valley results **75**
4.6.1 Conical valley, 10 degrees 75
4.6.2 Summary of results for various conical valley configurations 80
4.7 Hill results **82**
4.7.1 Triangular hill 82
4.7.2 Summary of results for various hill configurations 86

5 CONCLUSIONS 89

6 RECOMMENDATIONS 92

7 REFERENCES AND BIBLIOGRAPHY 94

APPENDICES

APPENDIX A - Journal articles

APPENDIX B - Shock detachment calculations

APPENDIX C - CNC machining method

APPENDIX D - Temperature graphs for developer

APPENDIX E - Experimental and Numerical images for valley and hill test pieces

APPENDIX F - Detailed Experimental and Numerical images for all valley and hill test pieces

LIST OF FIGURES

Figure 1.1: Supersonic F/A18 Hornet aircraft creates a condensation cloud as it accelerates through the sound barrier..... 2
Figure 1.2: Schlieren images of F-18 at M 1.4..... 2
Figure 1.3: Schematic of unsteady normal shock wave. 3
Figure 1.4: Schematic drawing of Regular reflection configuration. 4
Figure 1.5: Schematic drawing of Mach reflection configuration..... 4
Figure 1.6: The seven regions that identify the different reflection processes of a shock wave over a double wedge. 6
Figure 1.7: Actual region and transition boundaries of the seven different reflection processes for an incident shock wave with $M_i = 1.29$ over a double wedge. 9
Figure 1.8: Schematic representation of the reflection over a wall consisting of a concave followed by a convex corner: a) Regular reflection b) Mixed regular and Mach reflection c) Mach reflection..... 11

Figure 2.1: Shock tube facility at the University of the Witwatersrand. 16
Figure 2.2: Cross-section of the shock tube illustrating contraction geometry and diaphragms... 17
Figure 2.3: Photographs of driver section of the shock tube. 18
Figure 2.4: Photograph of expansion chamber of the shock tube..... 19
Figure 2.5: Photograph of test section of the shock tube..... 20
Figure 2.6: Photograph of the data acquisition system of the shock tube 21
Figure 2.7: Z-type schlieren arrangement..... 25
Figure 2.8: Photographs of the schlieren optical system. 26
Figure 2.9: Schematic representation of a supersonic aircraft entering a valley 27
Figure 2.10: Rectangular valley test pieces 28
Figure 2.11: Triangular valley test pieces 28
Figure 2.12: Graphical representation of the parabolic valley geometries 29
Figure 2.13: Parabolic valley test pieces 29
Figure 2.14: Graphical representation of the conical valley geometries 30
Figure 2.15: Conical valley test pieces 30
Figure 2.16: Rectangular valley test piece ($\theta_w = 60^o$, $\theta_v = 0^o$) with glass insert 31
Figure 2.17: Triangular, parabolic and conical hill test pieces..... 31

Figure 4.1: Schlieren images for rectangular valley, $\theta_w = 60^o$, $\theta_v = 0^o$, at time delay 1655μs, 1665μs, 1675μs, 1685μs, 1695μs, 1705μs, 1715μs, 1725μs and 1735μs respectively..... 40
Figure 4.2: Shadowgraph images for rectangular valley, $\theta_w = 60^o$, $\theta_v = 0^o$, at time delay 1660μs, 1670μs and 1680μs respectively..... 40
Figure 4.3: Time sequential density contour plots for rectangular valley, $\theta_w = 60^o$, $\theta_v = 0^o$. 41
Figure 4.4: Density contour plots for rectangular valley, $\theta_w = 60^o$, $\theta_v = 0^o$, taken in the y-z plane at x = 0mm, 18.75mm, 37.5mm, 42.5mm, 47.5mm, 52.5mm, 57.5mm, 62.5mm, 68.75mm, 75mm respectively..... 42
Figure 4.5: Enlarged density contour plots for rectangular valley, $\theta_w = 60^o$, $\theta_v = 0^o$, taken in the y-z plane at x = 40mm, 42.5mm, 47.5mm, 52.5mm, 57.5mm, 62.5mm respectively. 43
Figure 4.6: Pressure contour plots (single level) of secondary reflected wave for rectangular valley, $\theta_w = 60^o$, $\theta_v = 0^o$, taken in the y-z plane at x = 0mm, 18.75mm, 37.5mm, 42.5mm, 47.5mm, 52.5mm, 57.5mm, 62.5mm, 68.75mm, 75mm respectively..... 44
Figure 4.7: Superimposed pressure contour plots (single level) of secondary reflected wave for rectangular valley, $\theta_w = 60^o$, $\theta_v = 0^o$. 44
Figure 4.8: Superimposed pressure contour plots (multiple levels) of secondary reflected wave for rectangular valley, $\theta_w = 60^o$, $\theta_v = 0^o$. 44
Figure 4.9: Isometric views of sequential density contour plots for rectangular valley, $\theta_w = 60^o$, $\theta_v = 0^o$, taken in the x-y in steps of 5mm along the z axis. 45
Figure 4.10: Isometric view of superimposed density contour plots for rectangular valley, $\theta_w = 60^o$, $\theta_v = 0^o$, taken in the x-y plane..... 46
Figure 4.11: Sequential density contour plots for rectangular valley, $\theta_w = 60^o$, $\theta_v = 0^o$, taken in the x-y plane in steps of 5mm along the z axis..... 46
Figure 4.12: Enlarged sequential density contour plots for rectangular valley, $\theta_w = 60^o$, $\theta_v = 0^o$, taken in the x-y in steps of 5mm along the z axis..... 46
Figure 4.13: Superimposed density contour plots for rectangular valley, $\theta_w = 60^o$, $\theta_v = 0^o$, taken in the x-y plane. 47
Figure 4.14: Filled density contour plot of a y-z plane for rectangular valley, $\theta_w = 60^o$, $\theta_v = 0^o$, illustrating shear layer. 47
Figure 4.15: Isometric view of superimposed planes for rectangular valley, $\theta_w = 60^o$, $\theta_v = 0^o$. 48
Figure 4.16: Three-dimensional NURBS model of rectangular valley, $\theta_w = 60^o$, $\theta_v = 0^o$. 49
Figure 4.17: Isometric view of superimposed planes for rectangular valleys. 53
Figure 4.18 Three-dimensional NURBS model of rectangular valleys..... 54

Figure 4.19: Schlieren images for triangular valley, $\theta_w = 60^o$, $\theta_v = 0^o$, at time delay 1700μs, 1725μs, 1750μs, 1775μs, and 1800μs respectively. 55
Figure 4.20: Sequential density contour plots for triangular valley, $\theta_w = 60^o$, $\theta_v = 0^o$. 56
Figure 4.21: Density contour plots for triangular valley, $\theta_w = 60^o$, $\theta_v = 0^o$, taken in the y-z plane at x = 0mm, 25mm, 35mm, 45mm, 50mm, 55mm, 60mm, 65mm, 70mm and 75mm respectively. 57
Figure 4.22: Pressure contour plots (single level) of secondary reflected wave for triangular valley, $\theta_w = 60^o$, $\theta_v = 0^o$, taken in the y-z plane at x = 0mm, 25mm, 35mm, 45mm, 50mm, 55mm, 60mm, 65mm, 70mm and 75mm respectively. 58
Figure 4.23: Superimposed pressure contour plots (single level) of secondary reflected wave for triangular valley, $\theta_w = 60^o$, $\theta_v = 0^o$. 58
Figure 4.24: Isometric views of sequential density contour plots for triangular valley, $\theta_w = 60^o$, $\theta_v = 0^o$, taken in the x-y in steps of 5mm along the z axis. 59
Figure 4.25: Isometric view of superimposed density contour plots for triangular valley, $\theta_w = 60^o$, $\theta_v = 0^o$, taken in the x-y plane. 59
Figure 4.26: Sequential density contour plots for triangular valley, $\theta_w = 60^o$, $\theta_v = 0^o$, taken in the x-y plane in steps of 5mm along the z axis. 59
Figure 4.27: Enlarged sequential density contour plots for triangular valley, $\theta_w = 60^o$, $\theta_v = 0^o$, taken in the x-y in steps of 5mm along the z axis. 60
Figure 4.28: Superimposed density contour plots for triangular valley, $\theta_w = 60^o$, $\theta_v = 0^o$, taken in the x-y plane. 60
Figure 4.29: Filled density contour plot of plane in y-z plane for triangular valley, $\theta_w = 60^o$, $\theta_v = 0^o$, illustrating shear layer. 61
Figure 30: Isometric view of superimposed planes for triangular valley, $\theta_w = 60^o$, $\theta_v = 0^o$. 61
Figure 4.31: Three-dimensional NURBS model of triangular valley, $\theta_w = 60^o$, $\theta_v = 0^o$. 62
Figure 4.32: Isometric view of superimposed planes for triangular valleys. 66
Figure 4.33 Three-dimensional NURBS model of triangular valleys. 67
Figure 4.34: Schlieren images for parabolic valley, a = 0.04, at time delay 1650μs, 1675μs, 1700μs, 1725μs, and 1750μs respectively. 68
Figure 4.35: Sequential density contour plots for parabolic valley, a = 0.04. 69
Figure 4.36: Density contour plots for parabolic valley, a = 0.04, taken in the y-z plane at x = 0mm, 15mm, 25mm, 35mm, 45mm, 55mm, 65mm, 75mm, respectively. 70
Figure 4.37: Superimposed pressure contour plots (single level) of secondary reflected wave for parabolic valley, a = 0.04. 71

Figure 4.38: Sequential density contour plots for parabolic valley, a = 0.04, taken in the x-y plane in steps of 5mm along the z axis. 71
Figure 4.39: Enlarged sequential density contour plots for parabolic valley, a = 0.04, taken in the x-y plane in steps of 5mm along the z axis..... 72
Figure 4.40: Superimposed density contour plots for parabolic valley, a = 0.04, taken in the x-y plane. 72
Figure 4.41: Isometric view of superimposed planes for parabolic valley, a = 0.04. 72
Figure 4.42: Isometric view of superimposed planes for parabolic valleys. 75
Figure 4.43: Schlieren images for conical valley, 10 degrees, at time delay 1650μs, 1675μs, 1700μs, 1725μs, and 1750μs respectively. 76
Figure 4.44: Sequential density contour plots for conical valley, 10 degrees. 77
Figure 4.45: Density contour plots for conical valley, 10 degrees, taken in the y-z plane at x = 0mm, 45mm, 50mm, 55mm, 60mm, 65mm, 70mm, 75mm, respectively. 78
Figure 4.46: Superimposed pressure contour plots (single level) of secondary reflected wave for conical valley, 10 degrees..... 78
Figure 4.47: Sequential density contour plots for conical valley, 10 degrees, taken in the x-y plane in steps of 5mm along the z axis. 79
Figure 4.48: Enlarged sequential density contour plots for conical valley, 10 degrees, taken in the x-y plane in steps of 5mm along the z axis..... 79
Figure 4.49: Superimposed density contour plots for conical valley, 10 degrees, taken in the x-y plane. 80
Figure 4.50: Isometric view of superimposed planes for conical valley, 10 degrees. 80
Figure 4.51: Isometric view of superimposed planes for conical valleys..... 82
Figure 4.52: Schlieren images for triangular hill, at time delay 1650μs, 1675μs, 1700μs, 1725μs, and 1750μs respectively. 83
Figure 4.53: Sequential density contour plots for triangular hill. 84
Figure 4.54: Density contour plots for triangular hill, taken in the y-z plane at x = 0mm, 45mm, 50mm, 55mm, 60mm, 65mm,70mm, 75mm, respectively..... 85
Figure 4.55: Sequential density contour plots for triangular hill, taken in the x-y plane in steps of 5mm along the z axis. 86
Figure 4.56: Isometric view of superimposed planes for triangular hill..... 86
Figure 4.57: Isometric view of superimposed planes for hill configurations. 88

LIST OF TABLES

Table 1.1: A summary of the seven different reflection processes that can occur over convex and concave double wedges. 8

NOMENCLATURE

RR	Regular reflection
MR	Mach reflection
IR	Irregular reflection
i	incident shock wave
r	reflected shock wave
R	reflection point
D_iMR	Direct-Mach reflection
S_tMR	Stationary Mach reflection
I_nMR	Inverse-Mach reflection
m	Mach stem
s	slipstream
T	triple point
vNR	von Neumann reflection
TRR	Transitioned Regular reflection
SMR	Single Mach reflection
DMR	Double Mach Reflection
TMR	Transitional Mach reflection
X	trajectory angle of the first triple point
X’	trajectory angle of the second triple point
ADC	analogue to digital converter
ADAM	Analogue Data Acquisition Memory
θ_w	wedge angle
θ_I	incident shock wave angle
θ_r	reflected shock angle
M_S	incident shock wave Mach number
M_I	incident shock wave Mach number in steady frame of reference
θ_v	valley inclination angles

DEFINITION OF AXES

Two-dimensional axes:

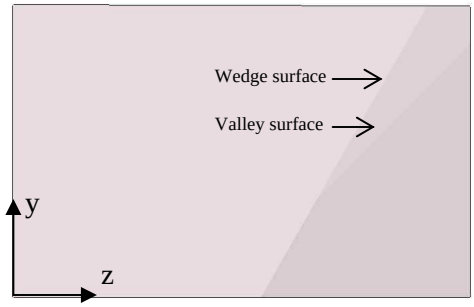

y-z plane



x-z plane

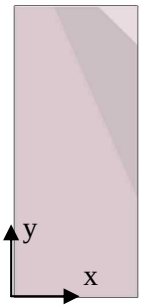

x-y plane

Three-dimensional axes:

